Synthesis, Structure, and Magnetic Properties of $SrLaMnSbO_6$: A New *B*-Site Ordered Double Perovskite

Tapas Kumar Mandal,[†] Artem M. Abakumov,[‡] Maxim V. Lobanov,[§] Mark Croft,[||] Viktor V. Poltavets,[†] and Martha Greenblatt*,[†]

Department of Chemistry and Chemical Biology and Department of Physics and Astronomy, Rutgers, The State University of New Jersey, Piscataway, New Jersey 08854, Department of Chemistry, Moscow State University, Moscow 119991, Russia, and R&D Department, Huntsman-NMG, Obninsk 249032, Russia

Received February 27, 2008. Revised Manuscript Received May 20, 2008

The synthesis, structural characterization, and magnetic property studies of $SrLaMnSbO_6$ double perovskite oxide are reported. The crystal structure of $SrLaMnSbO_6$ has been solved by powder X-ray (PXD) and neutron diffraction (NPD) data in the monoclinic space group $P2_1/n$ ($a = 5.6878(3)$ Å, $b = 5.6990(2)$ Å, $c = 8.0499(4)$ Å and $\beta = 89.98(2)°$; 295 K, NPD data). The Mn and Sb atoms are nearly completely ordered over the *B*-site of the perovskite structure. The octahedral framework displays significant tilting distortion according to the Glazer's tilt system $a^-a^-c^+$. X-ray absorption near-edge spectroscopic (XAS) studies show the presence of Mn^{2+} and Sb^{5+} formal oxidation states. The magnetic susceptibility data of $SrLaMnSbO_6$ indicate the presence of ferromagnetic correlations; the calculated effective paramagnetic moment, $\mu_{calcd} = 5.92\ \mu_B$ (for HS $Mn^{2+}(3d^5)$, $S = 5/2$; as evidenced by XAS data) is in good agreement with the value obtained experimentally ($\mu_{exp} = 5.70\ \mu_B$). Variable temperature neutron diffraction data show no evidence of structural transition down to 3.7 K. A long-range antiferromagnetic ordering is established at $T_N = 8$ K as evidenced by the magnetic susceptibility and specific heat measurements. The magnetic structure at 3.7 K is characterized by $\mathbf{k} = 0$ propagation vector and $m_{1x} = -m_{2x}$, $m_{1y} = m_{2y} = 0$, $m_{1z} = -m_{2z}$ ($m_x = 1.26(7)\ \mu_B$, $m_z = 1.82(6)\ \mu_B$) coupling of magnetic moments on the Mn_1 (1/2,0,0) and Mn_2 (0,1/2,1/2) atoms with the ordered magnetic moment of 2.21(4) μ_B.

1. Introduction

Double perovskite oxides ($A_2BB'O_6$) with a 1:1 rock-salt type of ordering[1] of the *B*-site cations are of paramount interest in solid state chemistry research, because of their interesting metallic/half-metallic ferromagnetic (FM) and magnetoresistive properties as observed in A_2FeMoO_6[2] and A_2FeReO_6[3] (A = Ca, Sr, Ba). Ordering of the transition metal ions (B and B') at the *B*-site of the perovskite structure plays a crucial role in determining their properties. Although it has been established that significant size and charge differences between the B and B' cations facilitate ordering at the *B*-site, other factors, such as, specific bonding interactions (e.g., Jahn−Teller distortions and polarization properties), synthesis condition, and formation temperature may affect the degree of order.[4]

Rock-salt type ordering is common among double perovskites and gives rise to diverse materials properties. For example, A_2FeMoO_6 and A_2FeReO_6 (A = Ca, Sr, Ba) are known to be ferri/ferromagnetic with critical temperatures (T_C's) in the range ~330−420 K.[5] Room-temperature magnetoresistance has been observed for Sr_2FeMoO_6 and Sr_2FeReO_6 because of intergrain tunneling.[2c,3d] The double perovskite family has been extensively revisited since the discovery of room-temperature half-metallicity and tunneling type magnetoresistance effect in Sr_2FeMoO_6 and Sr_2FeReO_6. Moreover, the recent discovery of magnetocapacitance and magnetoresistance (magnetodielectric effect) near room temperature in a FM semiconductor, La_2NiMnO_6,[6] has driven the field in search for new materials with exotic and useful properties.

Apart from the previous examples with two magnetic *B*-site cations, there exists another class of double perovskites

* To whom correspondence should be addressed. E-mail: martha@rutchem.rutgers.edu. Tel: (732) 445 3277. Fax: (732) 445 5312.
[†] Department of Chemistry and Chemical Biology, Rutgers, The State University of New Jersey.
[‡] Moscow State University.
[§] Huntsman-NMG.
[||] Department of Physics and Astronomy, Rutgers, The State University of New Jersey.

(1) (a) Anderson, M. T.; Greenwood, K. B.; Taylor, G. A.; Poeppelmeier, K. R. *Prog. Solid State Chem.* **1993**, *22*, 197. (b) Galasso, F.; Katz, L.; Ward, R. *J. Am. Chem. Soc.* **1959**, *81*, 820. (c) Galasso, F.; Darby, W. *J. Phys. Chem.* **1962**, *66*, 131.
(2) (a) Patterson, F. K.; Moeller, C. W.; Ward, R. *Inorg. Chem.* **1963**, *2*, 196. (b) Nakagawa, T. *J. Phys. Soc. Jpn.* **1968**, *24*, 806. (c) Kobayashi, K.-I.; Kimura, T.; Sawada, H.; Terakura, K.; Tokura, Y. *Nature (London)* **1998**, *395*, 677.
(3) (a) Longo, J.; Ward, R. *J. Am. Chem. Soc.* **1961**, *83*, 2816. (b) Sleight, A. W.; Weiher, J. F. *J. Phys. Chem. Solids* **1972**, *33*, 679. (c) Abe, M.; Nakagawa, T.; Nomura, S. *J. Phys. Soc. Jpn.* **1973**, *35*, 1360. (d) Kobayashi, K.-I.; Kimura, T.; Sawada, H.; Terakura, K.; Tokura, Y. *Phys. Rev. B* **1999**, *59*, 11159. (e) Gopalakrishnan, J.; Chattopadhyay, A.; Ogale, S. B.; Venkatesan, T.; Greene, R. L.; Millis, A. J.; Ramesha, K.; Hannoyer, B.; Marest, G. *Phys. Rev. B* **2000**, *62*, 9538.
(4) (a) Woodward, P.; Hoffmann, R.-D.; Sleight, A. W. *J. Mater. Res.* **1994**, *9*, 2118. (b) Shimada, T.; Nakamura, J.; Motohashi, T.; Yamauchi, H.; Karppinen, M. *Chem. Mater.* **2003**, *15*, 4494.
(5) Galasso, F.; Douglas, F. C.; Kasper, R. *J. Chem. Phys.* **1966**, *44*, 1672.
(6) Rogado, N. S.; Li, J.; Sleight, A. W.; Subramanian, M. A. *Adv. Mater.* **2005**, *17*, 2225.

10.1021/cm800583e CCC: $40.75
Published on Web 06/25/2008

where one of the *B*-site cation is nonmagnetic. For example, the synthesis and lattice parameters of the double perovskites Sr_2CrSbO_6 and Sr_2FeSbO_6 were reported in 1964 by Sleight and Ward.[7] Later, their detailed crystal structure and magnetic properties have been studied.[8] In their initial work, Battle et al.[8b] indicated establishment of a magnetically frustrated state for Sr_2FeSbO_6 at 36 K from magnetic susceptibility data[8b] and subsequently concluded the coexistence of magnetically ordered state with type I structure and a spin-glass system by neutron diffraction studies.[8c] Interestingly, in the analogous Sr_2FeBiO_6 with Bi^{5+} as the nonmagnetic *B*-cation, Byeon et al.[9] have demonstrated antiferromagnetic (AFM) ordering at a relatively high temperature (T_N = 91 K) by magnetic susceptibility and Mössbauer investigations.

The introduction of nonmagnetic cations at the *B*-site often leads to insulating and antiferromagnetic (AFM) materials.[8a] For example, in Mn-containing Sr_2MnMoO_6,[10] where Mo(VI) is the nonmagnetic *B*-site cation, insulating behavior with a Néel temperature (T_N) of 12 K is observed. Similarly, in A_2MnWO_6 (A = Ca, Sr)[10b,11] with $Mn^{2+}(d^5)$ and nonmagnetic $W^{6+}(d^0)$ at the *B*-sites, low-temperature AFM ordering has been confirmed by sequential NPD analysis. In Ca_2MnWO_6, Azad et al.[11] has substantiated the AFM state by magnetization studies as well. Moreover, it has been recognized that the magnetic sublattice of a 1:1 rock salt ordered double perovskite resembles a classical face centered cubic (fcc) lattice based on edge-shared tetrahedral network and such an AFM fcc lattice is geometrically frustrated.[12] Systems with geometrically frustrated exchange interactions are known to result in reduced magnetic ordering temperatures and moments as observed in Sr_2BReO_6 (B = Ca, Mg)[13] and (LaA)CoNbO$_6$ (A = Ca, Sr, Ba).[14] Furthermore, it must be mentioned that differing degrees of structural disorder on the *B*-sublattice could significantly alter the properties of double perovskites from those discussed above.

Recently, there has been renewed interest in Sr_2MnSbO_6 because of the report (Cheah et al.)[15] of cation ordering in this material when prepared at lower temperatures than that employed earlier by Lufaso et al.,[16] who reported a completely disordered structure for this material. In a subsequent study,[17] we have shown that Sr_2MnSbO_6 can be only partially ordered by careful control of its synthesis conditions. Interestingly, the chromium analogues, Ca_2CrSbO_6 and Sr_2CrSbO_6, form with an almost completely ordered array of CrO_6 and SbO_6 octahedra and exhibit FM and AFM orderings at low temperatures, respectively.[18] To increase the size and charge difference between Mn and Sb to force ordering and concurrent change in the physical properties, we have investigated the substitution of one Sr by La in Sr_2MnSbO_6. We expect that the heterovalent replacement of Sr^{2+} by La^{3+} must reduce the formal valence of the Mn cations (from 3+ to 2+) rather than that of the Sb ones, thus promoting *B*-site ordering. Indeed, the coexistence of Mn^{2+} and Sb^{5+} is common and was found before in a series of complex oxides: $MnSb_2O_6$,[19] $Mn_2Sb_2O_7$,[20] $Pb_5Sb_2MnO_{11}$,[21] $(Sb_{1-x}Pb_x)_2(Mn_{1-y}Sb_y)O_4$.[22] Moreover, an analogous Ta-series, ALaMnTaO$_6$ (A = Sr, Ba)[23] of the envisaged Sb compound has been reported to be formed in the ordered double perovskite structure. The details of synthesis, crystal and magnetic structure and magnetic properties of SrLaMnSbO$_6$ double perovskite are reported in this paper.

2. Experimental Section

Polycrystalline samples of SrLaMnSbO$_6$ were synthesized by solid state reactions from high purity (≥99.9% Aldrich, or Alfa Aesar) stoichiometric quantities of $SrCO_3$, La_2O_3, $MnC_2O_4 \cdot 2H_2O$, and Sb_2O_3. $SrCO_3$ and La_2O_3 were dried at 200 and 950 °C, respectively, prior to use. The starting materials were intimately ground, placed in an alumina boat, and heated under a controlled argon atmosphere in a tube furnace over a period of several days. The reaction mixture was first heated at 900 °C for 24 h, and the temperature was then raised in 100 °C steps to 1200 °C for 24−48 h each; finally, at 1250 °C, it was heated for 48 h until no further change was observed in the powder X-ray diffraction (PXD) patterns. The sample was thoroughly reground at each intermediate step and slow cooled to room temperature.

The PXD patterns were recorded at room temperature on a Bruker D8-Advance diffractometer (in Bragg−Brentano geometry with Cu Kα radiation, λ = 1.5418 Å) equipped with a SOL-X solid-state detector. For the structure refinements, the PXD data were collected in the angular range 10−120° in steps of 0.02° and with

(7) Sleight, A. W.; Ward, R. *Inorg. Chem.* **1964**, *3*, 292.
(8) (a) Blasse, G. *Philips Res. Rept.* **1965**, *20*, 327. (b) Battle, P. D.; Gibb, T. C.; Herod, A. J.; Hodges, J. P. *J. Mater. Chem.* **1995**, *5*, 75. (c) Cussen, E. J.; Vente, J. F.; Battle, P. D.; Gibb, T. C. *J. Mater. Chem.* **1997**, *7*, 459. (d) Kashima, N.; Inoue, K.; Wada, T.; Yamaguchi, Y. *Appl. Phys. A: Mater. Sci. Process.* **2002**, *74*, S805.
(9) Byeon, S. H.; Nakamura, T.; Itoh, M.; Matsuo, M. *Mater. Res. Bull.* **1992**, *27*, 1065.
(10) (a) Itoh, M.; Ohta, I.; Inaguma, Y. *Mater. Sci. Eng., B* **1996**, *41*, 55. (b) Muñoz, A.; Alonso, J. A.; Casais, M. T.; Martínez-Lope, M. J.; Fernández-Díaz, M. T. *J. Phys.: Condens. Matter* **2002**, *14*, 8817.
(11) Azad, A. K.; Ivanov, S. A.; Eriksson, S.-G.; Eriksen, J.; Rundlöf, H.; Mathieu, R.; Svedlindh, P. *Mater. Res. Bull.* **2001**, *36*, 2485.
(12) (a) Ramirez, A. P. *Annu. Rev. Mater. Sci.* **1994**, *24*, 453. (b) Greedan, J. E. *J. Mater. Chem.* **2001**, *11*, 37. (c) Karunadasa, H.; Huang, Q.; Ueland, B. G.; Schiffer, P.; Cava, R. J. *Proc. Natl. Acad. Sci. U.S.A.* **2003**, *100*, 8097.
(13) (a) Wiebe, C. R.; Greedan, J. E.; Luke, G. M.; Gardner, J. S. *Phys. Rev. B* **2002**, *65*, 144413. (b) Wiebe, C. R.; Greedan, J. E.; Kyriakou, P. P.; Luke, G. M.; Gardner, J. S.; Fukaya, A.; Gat-Malureanu, I. M.; Russo, P. L.; Savici, A. T.; Uemura, Y. J. *Phys. Rev. B* **2003**, *68*, 134410.
(14) Bos, J-W. G.; Attfield, J. P. *Phys. Rev. B* **2004**, *70*, 174434.
(15) Cheah, M.; Saines, P. J.; Kennedy, B. J. *J. Solid State Chem.* **2006**, *179*, 1775.
(16) Lufaso, M. W.; Woodward, P. M.; Goldberger, J. *J. Solid State Chem.* **2004**, *177*, 1651.
(17) Mandal T. K.; Poltavets, V. V.; Croft, M.; Greenblatt, M. *J. Solid State Chem.* **2008**, accepted.
(18) Retuerto, M.; Garcia-Hernandez, M.; Martinez-Lope, M. J.; Fernandez-Dias, M. T.; Attfield, J. P.; Alonso, J. A. *J. Mater. Chem.* **2007**, *17*, 3555.
(19) Vincent, H.; Turrillas, X.; Rasines, I. *Mater. Res. Bull.* **1987**, *22*, 1369.
(20) Scott, H. G. *Z. Kristallogr.* **1990**, *190*, 41.
(21) Abakumov, A. M.; Rozova, M. G.; Chizhov, P. S.; Antipov, E. V.; Hadermann, J.; Van Tendeloo, G. *J. Solid State Chem.* **2004**, *177*, 2855.
(22) Abakumov, A. M.; Rozova, M. G.; Antipov, E. V.; Hadermann, J.; Van Tendeloo, G.; Lobanov, M. V.; Greenblatt, M.; Croft, M.; Tsiper, E. V.; Llobet, A.; Lokshin, K. A.; Zhao, Y. *Chem. Mater.* **2005**, *17*, 1123.
(23) Horikubi, T.; Watanabe, H.; Kamegashira, N. *J. Alloys Compd.* **1998**, *274*, 122.

a step time of 9 s. The refinement of crystal structure from PXD data was performed by the Rietveld method with the FULLPROF program.[24]

Neutron powder diffraction (NPD) data were collected with the high-resolution BT-1 32 detector neutron powder diffractometer at the NIST Center for Neutron Research (NCNR), NBSR. A Cu(311) monochromator with a 90° takeoff angle, $\lambda = 1.5403(2)$ Å, and in-pile collimation of 15 min of arc were used. Data were collected over the range of 3−168° 2θ with a step size of 0.05°. The data collection time was approximately 8 h for each temperature and collected after equilibration for 0.5 h. The sample was contained in a 0.375 in. diameter vanadium can, which was slightly more than half-full. The instrument is described in the NCNR WWW site (http://www.ncnr.nist.gov/). The refinement of crystal and magnetic structure from NPD data was performed by the Rietveld method with the GSAS/EXPGUI program.[25]

Thermogravimetric analyses (TGA) were carried out with a TA Instruments 2050 thermal analyzer. Samples were heated at a rate of 5 °C/min under ambient air and 10% H_2−Ar mixture to a final temperature of 900 °C and cooled to room temperature under the same reaction atmosphere that was used during heating.

Magnetization data were collected with a Quantum Design MPMS-*XL* superconducting quantum interference device (SQUID) magnetometer. Temperature-dependent magnetization data were recorded at various applied magnetic fields (H) in the temperature range $2 < T\,(\mathrm{K}) < 400$ after cooling the sample in zero magnetic field (zero-field-cooled, ZFC) and while cooling in the presence of the field (field-cooled, FC). Measurements of magnetization (M) as a function of H were made at 5, 90, 200, and 300 K over the magnetic field ranges $-50 \le H\,(\mathrm{kOe}) \le 50$.

The Mn−K XAS measurement was performed in the fluorescence and transmission mode on a powdered sample on beam line X-19A at the Brookhaven National Synchrotron Light Source with methods discussed in the literature.[26,27] Briefly, the procedure that was used is the following. The incident and transmitted beam intensities were measured with ionization chambers and the fluorescence intensities with Canberra PIPS detectors. The absolute energy calibration was set to the elemental edge (first inflection point). The relative energy scale was maintained to better than ±0.05 eV with the simultaneously run standards.

In view of the low energy and strong "white line" s-to-p transition feature, the Sb−L_1 edge was measured in the total electron yield mode.[28] Here the "white line" (WL) terminology is conventional and refers to an atomic-like dipole transition into empty states, which typically manifests a sharply peaked near edge structure, which in prior years would leave a white-line-streak on photographic film. Such total-electron-yield measurements prevent finite sample thickness rounding out the white line feature; while still provide a bulk XAS spectrum.[28] Because a simultaneous standard was not possible in the total-electron-yield mode, an elemental standard, run before and after the sample, was used and the relative energy was ±0.1 eV or better.

As is routinely done, the spectra had a linear background subtracted (determined over ~80 eV interval below the edge), and were normalized to unity absorption step height across the edge.

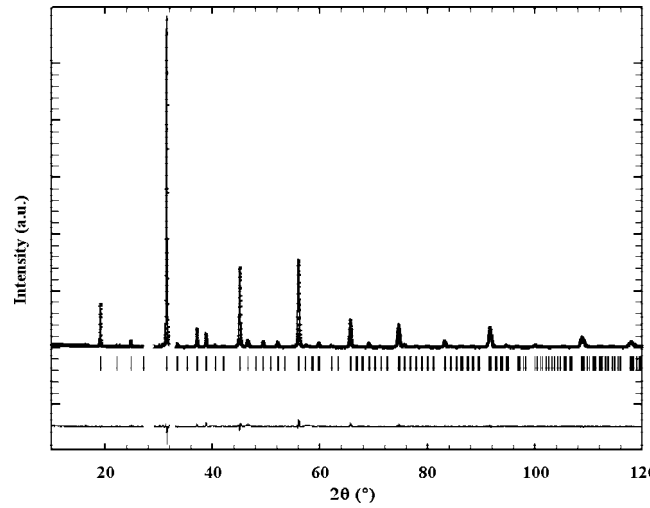

Figure 1. Rietveld refinement of $SrLaMnSbO_6$ from the PXD data. Observed (+), calculated (line), and difference (bottom) profiles are shown. The Bragg reflection positions are marked with vertical bars.

Here, an average of the data in ~50−200 eV range above the edge was used to set the normalization value.

The specific heat measurement was carried out in a Quantum Design PPMS. The data were collected upon warming after zero-field cooling.

3. Results and Discussion

3.1. Synthesis and Preliminary X-ray Characterization. $SrLaMnSbO_6$ was obtained as a black polycrystalline powder. The PXD pattern was characteristic of a double perovskite structure. A close analysis of the PXD pattern however indicated a small amount of La_3SbO_7 (JCPDS PDF #23−1138) as an impurity phase. The observed (by TGA analysis) and calculated weight losses are in fairly good agreement with the composition as derived from NPD (see later).

Rietveld refinement (Figure 1) of the structure of $SrLaMnSbO_6$ with the laboratory powder X-ray diffraction (PXD) data was carried out in the monoclinic space group $P2_1/n$. The refinement indicated nearly complete ordering (with ~2% disorder) of Mn and Sb at the B-site. The most intense peak regions due to La_3SbO_7 were excluded from the refinement (Figure 1). The refinement resulted the cell parameters of $a = 5.6849(5)$ Å, $b = 5.6934(4)$ Å, $c = 8.0400(7)$ Å, and $\beta = 90.02(1)^{\circ}$.

3.2. X-ray Absorption Spectra. The Mn−K edge of $SrLaMnSbO_6$ along with other standard compounds is shown in Figure 2a. The Mn−K edge of $SrLaMnSbO_6$ has been compared with other octahedrally coordinated standards, including MnO with the NaCl structure and a series of Mn-containing compounds with simple and double perovskite structures. The chemical shift of the K-edge for $SrLaMnSbO_6$ is highly consistent with the assignment of a Mn^{2+} formal valence state. As will be noted later in the magnetic results section, there is a high energy shoulder (see "S" in Figure 2a) on the main peak of the $SrLaMnSbO_6$ spectrum. The position of this broad S-feature would be consistent with some small fraction of Mn^{3+} admixture in the material. It should be noted, however, that the solid-state 4p orbital splittings could also cause this effect.

(24) Rodriguez-Carvajal, J. *Physica B* **1993**, *192*, 55.
(25) Larson, A. C.; Von Dreele, R. B. *General Structure Analysis System (GSAS)*, Los Alamos National Laboratory Report LAUR 86-748; Los Alamos National Laboratory: Los Alamos, NM, 2004.
(26) Tranquada, J. M.; Heald, S. M.; Moodenbaugh, A. R.; Liang, G.; Croft, M. *Nature (London)* **1989**, *337*, 720.
(27) Croft, M.; Sills, D.; Greenblatt, M.; Lee, C.; Cheong, S.-W.; Ramanujachary, K. V.; Tran, D. *Phys. Rev. B* **1997**, *55*, 8726.
(28) (a) Guo, T.; DenBoer, M. *Phys. Rev. B* **1985**, *31*, 6233. (b) Jeon, Y.; Chen, J.; Croft, M. *Phys. Rev. B* **1994**, *50*, 6555.

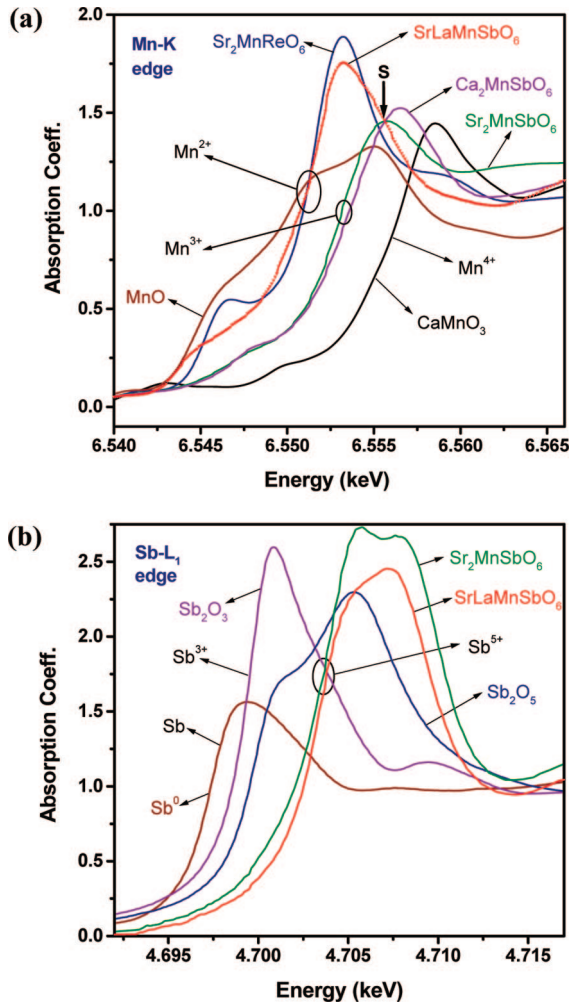

Figure 2. XAS data for $SrLaMnSbO_6$ along with other materials used as standards at the (a) Mn−K and (b) Sb−L_1 edge.

As a p-block element the frontier bonding orbital of Sb are the 5p states with the 5s states being involved in the higher valence state. The Sb−L_1 near-edge spectra of $SrLaMnSbO_6$ along with some standards and previously studied compounds are shown in Figure 2b. The elemental Sb−L_1 spectrum manifests a broad peak due to 2s core transitions into the three empty 5p states (as always, a step feature due to the onset of 2s to continuum transitions is also present). The Sb^{3+} standard Sb_2O_3 spectrum shows a dramatic chemical shift to higher energy, an increase in the intensity and narrowing (in energy) of the WL 5p feature. The increase in intensity is consistent with the greater number of 5p holes, and the narrowing is consistent with the more localized atomic character in the higher valance state (which also enhances the transition matrix element). The centrum of the WL peak feature of the Sb^{5+} standard, Sb_2O_5 spectrum exhibits a clear shift to higher energy and the development of a higher energy second peak. The Sb−L_1 spectrum of $SrLaMnSbO_6$ is remarkable in that the WL-feature is quite narrow and strongly shifted to higher energy. Indeed, it compares very well with Sr_2MnSbO_6, which constitutes a better Sb^{5+} XAS standard than does the binary oxide.[17] The Sb^{5+} valence state in $SrLaMnSbO_6$ is abundantly clear from the Sb−L_1 edge measurements.

3.3. Magnetic Properties. The thermal evolution of the susceptibility (M/H) and inverse susceptibility (H/M) data are shown in Figure 3. The susceptibility (Figure 3a) exhibits a steady rise below 250 K, followed by a plateaulike region at ∼50−100 K, and finally, a cusp at ∼10 K. The magnetization has strong field dependence and shows significant differences between the FC and ZFC data at low field strengths. The inverse susceptibility data (Figure 3b) show substantial nonlinearity over the entire temperature range. The high temperature (300−400 K region) region of the 1000 Oe data can be fitted with a Curie−Weiss (CW) law with positive Weiss constant ($\theta_W = 62$ K), which indicates the dominance of ferromagnetic correlations in the system. The effective paramagnetic moment of 5.70 μ_B is slightly lower than that calculated, 5.92 μ_B (assuming Mn^{2+}, d^5, $S = 5/2$) and very close to the value obtained for divalent Mn in MnO.[29]

The magnetic behavior below 300 K (especially, the nonlinear magnetization, Figure 4) indicates the presence of FM clusters. However, no ordered magnetic moment is found by analysis of the NPD data for all data sets above 3.7 K (see below): the observed intensities can be adequately fitted with only the crystallographic model (as described below), so the observed FM correlations should be short-range only. It is possible that the origin of the observed FM correlations is related to the antisite defects (approximately 5% of Mn at Sb site is found by NPD, see below). The low magnitude of the nonlinear rise without any hysteresis (superparamagnetic-like) in the magnetization (see Figure 4) below 1000 Oe clearly supports such a low concentration scenario.

According to the NPD refinement, the composition is $SrLaMn_{1.05}Sb_{0.95}O_6$, which corresponds to the formal Mn valence +2.14. The Mn atoms in an antisite (at Sb site) would probably have Mn^{3+} admixtures. Indeed, in the discussion of Mn−K edge XAS (see Figure 2a), the S-shoulder feature was noted to be consistent with some Mn^{3+} admixture in this material. This Mn^{3+} admixture could give rise to a local double exchange Mn^{2+}−O−Mn^{3+} interaction with all of the sites surrounding the antisite leading to a FM cluster. Such a stabilized local cluster could have canted AFM interactions in the next more distant cell which could further enhance the cluster stability correlations.

In this respect, the striking similarity of the inverse susceptibility (H/M) curves (see Figure 3b) to those observed in a ferromagnetic material should be noted. Here, the FM core of the cluster with an AFM correlated shell would have a local ferromagnetic character. The canting in such correlated regions, however, if present, would enhance the FM response.

On the other hand, if at $T \approx 300$ K, AFM 180° Mn−O−Mn superexchange correlations set in, then local AFM domains could possess a net FM component from canting of AFM sublattices. The symmetry analysis of the magnetic configurations for the $P2_1/n$ space group (see below) does allow for such an AFM canting. However, this possibility would result in a very low magnitude of the FM contribution and furthermore is not supported by evidence

(29) Tyler, R. W. *Phys. Rev.* **1933**, *44*, 776.

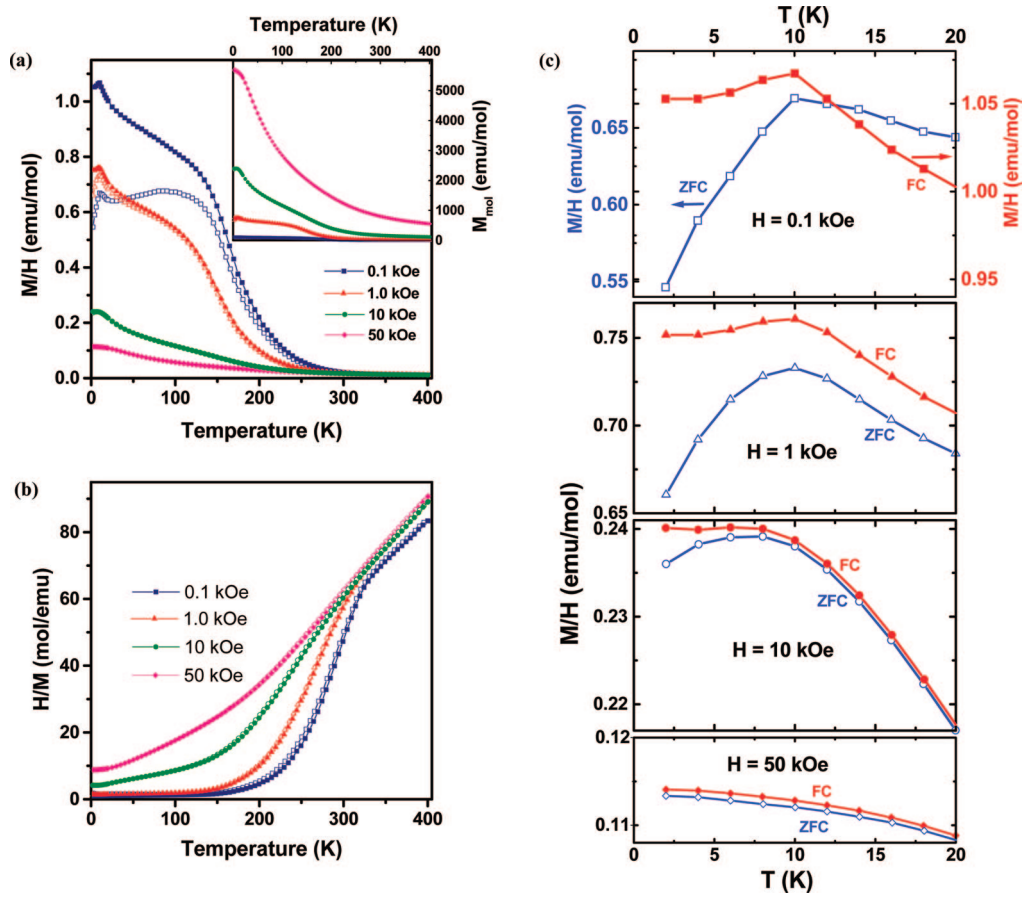

Figure 3. Temperature dependence of field-cooled (filled symbols) and zero-field-cooled (open symbols) (a) molar susceptibility (M/H) and (b) inverse molar susceptibility (H/M) data measured at 0.1, 1.0, 10, and 50 kOe for $SrLaMnSbO_6$. In (c), the M/H curves across the onset of magnetic order below 20 K are shown on an expanded scale. The inset in (a) shows the temperature dependence of molar magnetization.

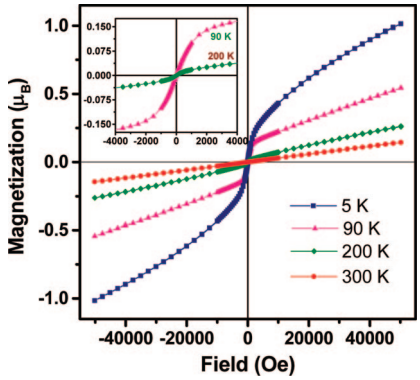

Figure 4. Magnetization versus field data of $SrLaMnSbO_6$ measured at 5, 90, 200, and 300 K. Inset shows the magnetization (on an expanded y-scale) up to ±4000 Oe for the 90 and 200 K data.

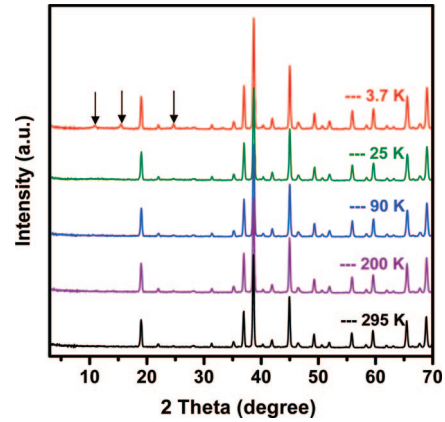

Figure 5. NPD patterns of $SrLaMnSbO_6$ at 3.7, 25, 90, 200, and 295 K. The appearance of magnetic reflections (indicated by arrows)/enhancement due to magnetic contributions is observed for the data at 3.7 K.

for substantial AFM canting in the NPD data analysis of the ordered state.

Considering the inherent geometric frustration operating in the magnetic Mn^{2+} sublattice and some percent of disorder present in this system, a more rigorous explanation about the magnetic properties is in order. The calculated frustration factor,[12,13] f ($f = |\theta|/T_N$), of 7.5 for $SrLaMnSbO_6$ indicates a fairly strong degree of geometric frustration. However, the small disorder present because of antisite defects (see NPD refinement) would disrupt the geometric frustration significantly. The low AFM ordering temperature (below 10 K) away from θ_W (62 K) and a much lower value for the ordered magnetic moment (as obtained from NPD analysis at 3.7 K, see later) than expected for Mn^{2+} (d^5) is attributed to the complex interplay between geometric frustration and disorder. It has also been mentioned previously[14] in the (LaA)-$CoNbO_6$ (A = Ca, Sr, Ba) system, where a decrease in T_N and reduction in saturation moment were attributed to magnetic frustration, which increases with the unit-cell symmetry. As the unit-cell symmetry increases, the competition between 90° superexchange pathways becomes dominant as the exchange strengths become comparable. However, the monoclinic distortion (see NPD data) in $SrLaMnSbO_6$ would

Table 1. Selected Parameters of the Rietveld Refinement for the $SrLaMn_{1.05}Sb_{0.95}O_6$ Structure from NPD data at $T = 3.7$ and 295 K

	T (K)	
	3.7	295
space group	$P2_1/n$	$P2_1/n$
a (Å)	5.6777(2)	5.6878(3)
b (Å)	5.6968(2)	5.6990(2)
c (Å)	8.0374(3)	8.0499(4)
β (deg)	89.989(8)	89.98(1)
cell volume (Å^3)	259.97(2)	260.94(2)
Z	2	2
calcd density (g/cm^3)	6.335	6.311
2θ range, step (deg)	$8.35 \le 2\theta \le 152.5$, 0.05	$8.35 \le 2\theta \le 152.5$, 0.05
χ^2, R_P, R_{wP}	1.395, 0.044, 0.056	1.33, 0.047, 0.059

lead to anisotropic exchange interactions and disrupt the ideal frustrated environment resulting in weaker glassiness. This is consistent with the disappearance of a well defined peak in susceptibility with higher magnetic fields and a broad anomaly in the heat capacity data (see below).

In Figure 3c, the M/H curves at temperatures below 20 K (spanning the onset of magnetic order) are displayed at various fields. The $H = 0.1$ and 1 kOe curves clearly manifest maxima near 10 K. The ZFC results have convex curvature below 10 K, whereas the FC curves (at these two lowest fields) manifest inflection points near 8 K. As will be revisited later, mean field theory predicts a peak in the low-field susceptibility, χ (M/H), at an AFM Néel temperature, whereas the inclusion of fluctuation effects in modeling (and real systems) places the transition temperature at the inflection point on the low-energy side of the peak. In many cases this difference can be small; however, in cases like the one at hand, where fluctuations are important (e.g., for ~2D systems, or where frustration, or other local disordering effects are relevant), it can be appreciable or even large. The low-field FC inflection points at 8 K are therefore here associated with the ordering temperature, a conclusion that will be supported below by the heat capacity measurements.

A couple of additional points should be noted. The ZFC measurements (in the ordered phase) involve a more complicated mix of initially randomly oriented domains, which will reorganize irreversibly as the ordering temperature is approached from below. The FC process allows for preferred magnetic domain growth through the transition and yields a clearer picture of the order parameter growth with decreasing temperature. In the higher-field $H = 10$ kOe curve (Figure 3c), the peak in M/H has been depressed to 8 K, indicating the presence of AFM correlations. Finally, at 50 kOe (Figure 3c), the maximum in the M/H curve is below the range of measurement. This could indicate the suppression of the AFM order or the presence of a spin-flopped state, in which the transition signature would be more difficult to analyze.

3.4. Neutron Powder Diffraction: Crystallographic and Magnetic Structure. The NPD pattern of the $SrLaMnSbO_6$ phase can be indexed based on a primitive cubic unit cell with $a = 8.0506(3)$ Å. However, the detailed profile analysis revealed significantly inadequate description of the peak shapes in both cubic and suitable tetragonal unit cells, which indicates that the actual symmetry is lower. When the data was indexed in an orthorhombic unit cell with the $a \approx a_p\sqrt{2}$, $b \approx a_p\sqrt{2}$, $c \approx 2a_p$, the observed extinction conditions correspond to the space group *Pbnm* that is characteristic for the *B*-site disordered double perovskite with the $a^-a^-c^+$ Glazer's tilt system. Attempt of the Rietveld refinement in the *Pbnm* model revealed large deviations between the observed and calculated intensities, which were completely eliminated by lowering the symmetry down to $P2_1/n$ with the ordered Mn and Sb cations maintaining the same tilt system. Two of the most intense admixture peaks were excluded from the refinement. The possibilities of deviations in chemical composition and antisite Mn/Sb disorder was verified by the refinement of the La/Sr ratio at the *A*-position and the Mn/Sb ratio at the 2d and 2a *B*-positions. The refined occupancy factors for the *A*-position and 2d *B*-position do not deviate in the range of one standard deviation from $g = 50\%$ La + 50% Sr and $g = 100\%$ Mn, respectively. A small amount of Mn was found together with the Sb atoms at the 2a position corresponding to $g = 95\%$ Sb + 5% Mn. Thus the chemical composition is slightly Mn-enriched corresponding to the formula, $SrLaMn_{1.05}Sb_{0.95}O_6$. Final refinement was performed with an isotropic approximation for the atomic displacement parameters (ADPs) and resulted in a good agreement between the experimental and calculated profiles.

The development of long-range magnetic ordering was monitored by comparing the NPD patterns taken at 3.7, 25, 90, 200, and 295 K (Figure 5). No noticeable changes in intensity of nuclear reflections and/or appearance of extra reflections was observed down to $T = 25$ K (Figure 5). Although our diffraction experiment was not optimized for small-angle neutron scattering (SANS), we examined the difference plots, i.e., the 295 K data were subtracted from that at 25 K (corrected for thermal expansion). We actually observed diffuse scattering around the positions of AFM reflections evidencing short-range AFM ordering when approaching T_N. However, the analysis of the low-Q region (minimum $Q = 0.21$ Å^{-1}) revealed no magnetic SANS features. From our NPD experiment, we could not directly rule out or confirm the presence of FM clusters.

However, a long-range magnetically ordered state is achieved only at 3.7 K, which is consistent with the observation of a cusp in the magnetic susceptibility at ~10 K (Figure 3). The reflections appearing in the low-angle region of the NPD pattern at 3.7 K can be indexed with $\mathbf{k} = 0$ propagation vector and correspond to AFM ordering. The representational analysis for the $P2_1/n$ space group and $\mathbf{k} = 0$, as reported in ref,[30] revealed the symmetry allowed magnetic structures. An adequate fit for the magnetic reflections was achieved for the magnetic structure corresponding to the Γ^1 irreducible representation (according to Kovalev's notation) with the magnetic moment components m_x,m_y,m_z for the Mn (1/2,0,0) atom and $-m_x,m_y,-m_z$ for the Mn (0,1/2,1/2) atom. A nonzero ferromagnetic component along the *b*-axis is allowed by symmetry. However, the refinement of the m_y component leads to the value close to zero with very large standard deviation revealing the insignificance of this parameter for the refinement. One can

(30) Augsburger, M. S.; Viola, M. C.; Pedregosa, J. C.; Munoz, A.; Alonso, J. A.; Carbonio, R. E. *J. Mater. Chem.* **2005**, *15*, 993.

Table 2. Structural Parameters for the SrLaMn$_{1.05}$Sb$_{0.95}$O$_6$ Structure from NPD data at T = 3.7 and 295 K

	T (K)	
	3.7	295
LaSr1, occupancy	4g, 0.5La + 0.5Sr	4g, 0.5La + 0.5Sr
x, y, z	0.5082(2), 0.5312(2), 0.2504(7)	0.5055(2), 0.5285(2), 0.2512(9)
U_{iso} (Å^2)	0.0056(2)	0.0127(3)
Mn1, occupancy	2d, Mn	2d, Mn
x, y, z	1/2, 0, 0	1/2, 0, 0
U_{iso} (Å^2)	0.0039(7)	0.0074(8)
m_x, m_y, m_z, (μ_B)	1.26(7), 0, 1.82(6)	
Sb1, occupancy	2a, 0.95Sb + 0.05Mn	2a, 0.95Sb + 0.05Mn
x, y, z	1/2, 0, 1/2	1/2, 0, 1/2
U_{iso} (Å^2)	0.0035(5)	0.0059(6)
O1, occupancy	4g, O	4g, O
x, y, z	0.2275(7), 0.2055(9), 0.5376(7)	0.228(1), 0.206(1), 0.538(1)
U_{iso} (Å^2)	0.007(1)	0.015(1)
O2, occupancy	4g, O	4g, O
x, y, z	0.2993(7), 0.721(1), 0.5420(7)	0.2983(9), 0.721(1), 0.540(1)
U_{iso} (Å^2)	0.013(1)	0.019(2)
O3, occupancy	4g, O	4g, O
x, y, z	0.4254(6), 0.9826(5), 0.2584(8)	0.4274(8), 0.9844(6), 0.259(1)
U_{iso} (Å^2)	0.0092(6)	0.0148(8)

Table 3. Main Interatomic Distances (Å) and Bond Angles (deg) for the SrLaMn$_{1.05}$Sb$_{0.95}$O$_6$ Structure at T = 3.7 and 295 K

T = 3.7 K		T = 295 K	
LaSr1−O1	2.508(6) × 1	LaSr1−O1	2.519(10) × 1
LaSr1−O1	2.722(7) × 1	LaSr1−O1	2.736(8) × 1
LaSr1−O1	2.852(7) × 1	LaSr1−O1	2.862(9) × 1
LaSr1−O2	2.459(7) × 1	LaSr1−O2	2.470(10) × 1
LaSr1−O2	2.744(6) × 1	LaSr1−O2	2.777(8) × 1
LaSr1−O2	2.840(7) × 1	LaSr1−O2	2.825(9) × 1
LaSr1−O3	2.478(3) × 1	LaSr1−O3	2.476(5) × 1
LaSr1−O3	2.615(3) × 1	LaSr1−O3	2.637(3) × 1
LaSr1−O3	3.161(3) × 1	LaSr1−O3	3.133(1) × 1
Mn1−O1	2.139(4) × 2	Mn1−O1	2.139(6) × 2
Mn1−O2	2.142(4) × 2	Mn1−O2	2.136(5) × 2
Mn1−O3	2.122(7) × 2	Mn1−O3	2.126(9) × 2
Sb1−O1	1.964(5) × 2	Sb1−O1	1.967(6) × 2
Sb1−O2	1.984(5) × 2	Sb1−O2	1.988(7) × 2
Sb1−O3	1.990(7) × 2	Sb1−O3	1.986(9) × 2
Mn1−O1−Sb1	157.2(3)	Mn1−O1−Sb1	157.3(4)
Mn1−O2−Sb1	154.1(3)	Mn1−O2−Sb1	155.0(4)
Mn1−O3−Sb1	155.5(2)	Mn1−O3−Sb1	156.3(2)

assume that the canting angle is negligibly small and the m_y component was fixed to zero in the final refinement. The refinement of the m_x and m_z components resulted in the net magnetic moment of 2.21(4) μ_B for the Mn^{2+} cations. The low value of the ordered magnetic moment reflects a significant degree of magnetic frustration in the system.

Selected parameters from the Rietveld refinement, atomic coordinates, occupancies and ADPs and main interatomic distances are listed in Tables 1, 2, and 3. Observed, calculated and difference NPD patterns at 3.7 and 295 K are shown in Figure 6. The crystal and magnetic structures of SrLaMn$_{1.05}$Sb$_{0.95}$O$_6$ are shown in Figure 7. The Mn^{2+} and Sb^{5+} cations are located at slightly distorted octahedra with the average Mn−O and Sb−O distances of 2.134 and 1.980 Å, which is in agreement with the ionic radii of these cations ($r(Mn^{2+})$ = 0.82 Å, $r(Sb^{5+})$ = 0.69 Å).[31] Corresponding to the low value of tolerance factor t = 0.88, the octahedral framework is strongly distorted as can be seen from the Mn−O−Sb bond angles (Table 3), which are much lower than 180 °. The tilt system corresponds to the Glazer's notation $a^-a^-c^+$.[32] The bond valence sum (BVS) values for the Mn^{2+} and Sb^{5+} cations of 2.37 and 5.41, respectively, substantially exceed the nominal values. This indicates that, in spite of the large degree of tilting distortion, the octahedral framework is under compressive strain in order to adopt reasonably short La−O and Sr−O distances. The global instability index of 0.142 calculated for the bond valence optimized SrLaMnSbO$_6$ structure with the SPuDS software is characteristic for a lattice-strained perovskite structure.[33,34]

The charge difference of 3 and size difference of 0.21 Å between Mn^{2+} and Sb^{5+} satisfy the criteria proposed by Anderson et al.[1] and appear to be sufficient to achieve complete ordering at the *B*-sublattice. Increasing the oxidation state of the Mn cations on going from SrLaMnSbO$_6$ to

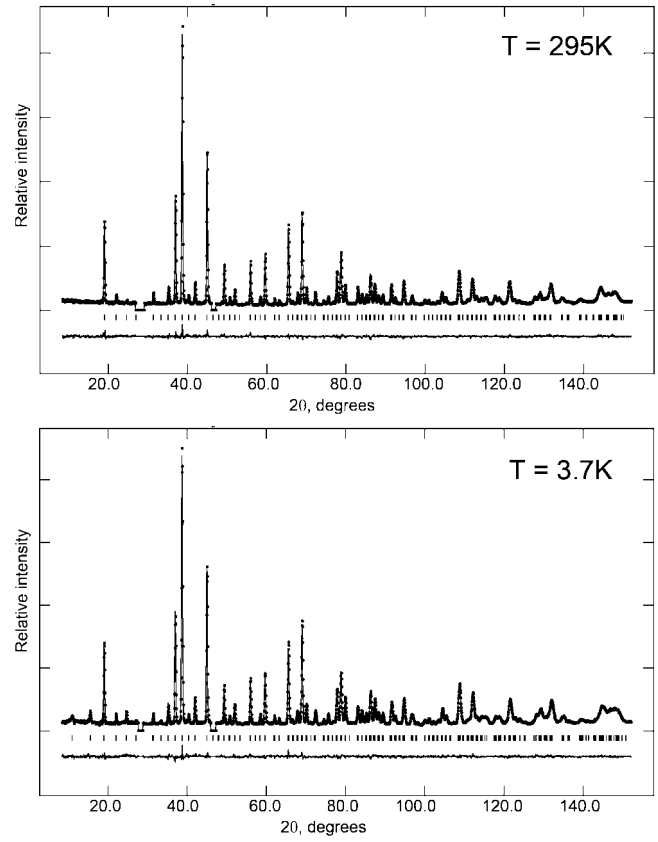

Figure 6. Observed (dots), calculated, and difference NPD patterns corresponding to the refinement of the SrLaMn$_{1.05}$Sb$_{0.95}$O$_6$ structure at T = 295 and 3.7 K.

(31) Shannon, R. D.; Prewitt, C. T. *Acta Crystallogr., Sect. B* **1969**, *35*, 745.

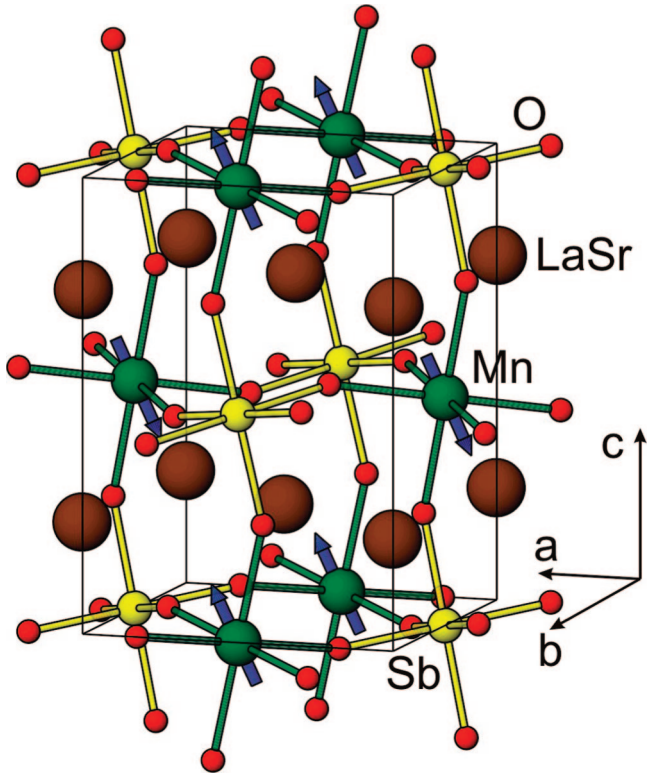

Figure 7. Crystal and magnetic structure of $SrLaMn_{1.05}Sb_{0.95}O_6$. The magnetic moments on the Mn atoms are shown as blue arrows.

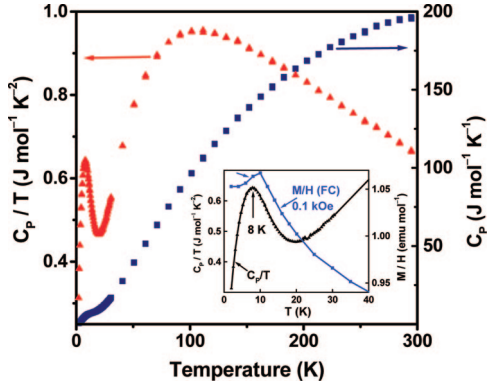

Figure 8. Temperature dependence of molar heat capacity (C_P) and C_P/T data for $SrLaMnSbO_6$. Inset shows the low-temperature C_P/T data along with the field-cooled $H = 0.1$ kOe M/H data on an expanded scale.

Sr_2MnSbO_6 reduces both charge and size difference that results in partial ordering of the Mn^{3+} and Sb^{5+} cations.[17] Further decrease of the charge difference in $CaRMn^{3+}Sn^{4+}O_6$ (R = La, Pr, Nd, Sm−Dy) double perovskites is accompanied by a complete disorder over the B-sublattice even in spite of Jahn−Teller distortion intrinsic in the Mn^{3+} cations.[35]

3.5. Heat Capacity. Figure 8 shows the temperature dependence of the molar heat capacity (C_P) and C_P/T data for $SrLaMnSbO_6$. At temperatures above 20 K, the large rise in C_P is dominated by the lattice-phonon contributions and is qualitatively consistent with a Debye type dependence with the high temperature limit very close to the Dulong−Petit value of $3R$. The quantitatively high-T C_P variation departs from a simple Debye form sufficiently that subtraction of the lattice contribution to extract a subtle magnetic contribution is not possible. Below 20 K, the lattice contributions are small enough to discuss the magnetic contributions.

There is a broad shoulder in C_P at low temperatures, which is much clearer in the C_P/T plot. The low temperature C_P/T data is shown on an expanded scale in the inset of Figure 8 along with the field-cooled $H = 0.1$ kOe M/H data. There is a clear peak anomaly (albeit broad compared to a robust magnetic ordering anomaly) in C_P/T at 8 K. The low-field magnetic susceptibility, χ (M/H), shows a peak at a somewhat higher temperature of ~10 K. Although within the mean field approximation the peak in χ occurs at the Néel temperature of an AFM, in real systems (and theories which take proper account of fluctuations) the value of T_N is known to be the inflection point on the low temperature side of the χ maximum. Indeed this inflection point in the FC-M/H curve is seen to coincide, within experimental uncertainties, in temperature with the peak in C_P/T. The transition temperature for the AFM order observed at 3.7 K in the NPD is therefore assigned the value of 8 K.

Integration of the entropy up to 20 K was found to be ~65% of the $S = 5/2$ value of $R\ln(6)$. Here, the use of a Debye T^3 background with a range of reasonable Debye temperatures did not appreciably alter this integrated value. The broadness of the specific heat anomaly, as well as the spin-cluster, frustration and glassy effects render the entropy shortfall expected.

4. Conclusion

A new double perovskite $SrLaMnSbO_6$ has been synthesized and its structure and magnetic properties have been investigated with powder X-ray and neutron diffraction, X-ray absorption spectroscopy, and magnetometry. The crystal structure, as evidenced by Rietveld refinement of the PXD and NPD data, is monoclinic ($P2_1/n$) consisting of almost completely ordered arrays of MnO_6 and SbO_6 octahedra. XAS clearly indicates Mn^{2+} and Sb^{5+} formal oxidation states in this material. Variable temperature NPD studies show no structural transition down to 3.7 K. While the magnetization data down to 90 K shows significant ferromagnetic correlations, the magnetic susceptibility data indicate long-range AFM ordering below $T_N = 10$ K. The NPD data at 3.7 K demonstrates an AFM ordered state, which is further supported by the specific heat anomaly observed at 8 K. Refinement of the magnetic structure at 3.7 K results in an ordered magnetic moment of 2.21(4) μ_B on the Mn^{2+} sites.

Acknowledgment. We acknowledge the support of the National Institute of Standards and Technology (NIST), U.S. Department of Commerce, in providing the neutron research facilities used in this work. T.K.M. and M.G. thank Dr. Judith K. Stalick for her help with the neutron data collection at BT-1, NCNR. This work was supported by the National Science Foundation, Solid State Chemistry Grants NSF-DMR-0233697 and NSF-DMR-0541911, and in part by the Russian Foundation of Basic Research (RFBR Grants 07-03-00664-a, 06-03-90168-a, and 05-03-34812-MF-a).

CM800583E

(32) Glazer, A. M. *Acta Crystallogr., Sect. B* **1972**, *28*, 3384.
(33) Salinas-Sanchez, A.; Garcia-Munoz, J. L.; Rodriguez-Carvajal, J.; Saez-Puche, R.; Martinez, J. L. *J. Solid State Chem.* **1992**, *100*, 201.
(34) Lufaso, M. W.; Woodward, P. M. *Acta Crystallogr., Sect. B* **2001**, *57*, 725.
(35) Abakumov, A. M.; Rossell, M. D.; Seryakov, S. A.; Rozova, M. G.; Markina, M. M.; Van Tendeloo, G.; Antipov, E. V. *J. Mater. Chem.* **2005**, *15*, 4899.